NANO LETTERS

Letter

pubs.acs.org/NanoLett

Nanochannel-Based Single Molecule Recycling

John F. Lesoine,[†] Prahnesh A. Venkataraman,[‡] Peter C. Maloney,[§] Mark E. Dumont,[‡] and Lukas Novotny*[,†]

[†]Institute of Optics, University of Rochester, Rochester, New York 14627, United States

[‡]Department of Biochemistry and Biophysics, University of Rochester Medical Center, Rochester, New York 14642, United States

[§]Department of Physiology, Johns Hopkins Medical School, Baltimore, Maryland 21205, United States

S *Supporting Information*

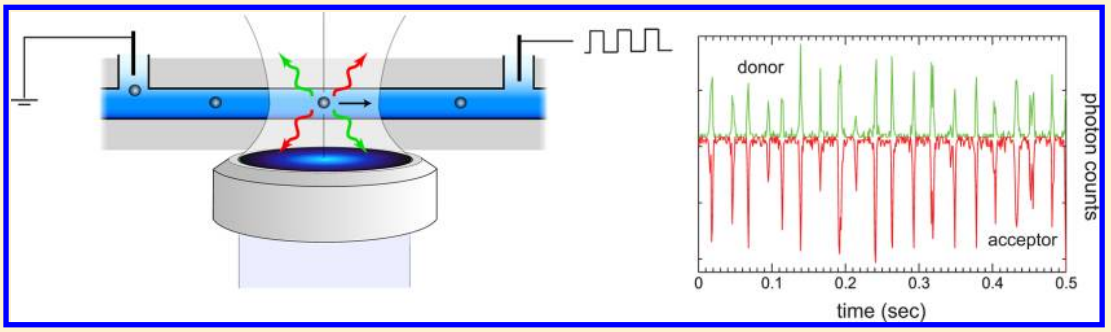

ABSTRACT: We present a method for measuring the fluorescence from a single molecule hundreds of times without surface immobilization. The approach is based on the use of electroosmosis to repeatedly drive a single target molecule in a fused silica nanochannel through a stationary laser focus. Single molecule fluorescence detected during the transit time through the laser focus is used to repeatedly reverse the electrical potential controlling the flow direction. Our method does not rely on continuous observation and therefore is less susceptible to fluorescence blinking than existing fluorescence-based trapping schemes. The variation in the turnaround times can be used to measure the diffusion coefficient on a single molecule level. We demonstrate the ability to recycle both proteins and DNA in nanochannels and show that the procedure can be combined with single-pair Förster energy transfer. Nanochannel-based single molecule recycling holds promise for studying conformational dynamics on the same single molecule in solution and without surface tethering.

KEYWORDS: *Single molecule detection, nanofluidics, trapping, FRET, electroosmosis*

While fluorescence spectroscopy of molecules in solutions provides precise measurements of population averages of relevant parameters, such measurements are generally not capable of providing insight into heterogeneity of molecular populations, fluctuations in molecular behavior, or the detailed kinetics of molecular transitions. The problems associated with ensemble averaging can be circumvented using single molecule fluorescence.[1−5] Single molecule experiments can be performed using molecules immobilized on surfaces[6−8] or diffusing in solution.[9,10] Immobilization generally involves modification of the molecules being studied to allow them to be attached to a surface. Both the modifications and the proximity to a surface can alter properties of the molecules being studied.[11] On the other hand, single molecule analyses of freely diffusing molecules are subject to limitations in the number of photons that can be collected that are imposed by Brownian motion of molecules diffusing through the laser focus.[12] A constant drift velocity combined with hydrodynamic focusing,[13,14] or mechanical confinement in channels or nanopipettes,[15] can reduce variations in photon counts by providing more constant transit times through the laser focus. However, these passive approaches still only allow observation times on the order of a few milliseconds. Therefore, it is important to develop immobilization-free methods that remove surface-specific artifacts and that increase measurement time compared to single molecule diffusion experiments.

Trapping molecules inside lipid vesicles that are tethered to a surface provides a method for localizing minimally modified molecules in the laser focus of a microscope;[16] however, this approach results in high effective concentrations of the target held in close proximity to a lipid bilayer.[17] While trapping in vesicles has provided useful single molecule analyses of some soluble proteins,[18] it complicates experiments requiring rapid changes of solution conditions and has limited applicability for other proteins and systems involving surfactants that would strongly interact with or disrupt membranes. This limitation can be overcome by methods based on active tracking and trapping, such as the anti-Brownian electrokinetic (ABEL) trap, which uses electrokinetic feedback to cancel Brownian diffusion, allowing individual fluorophores and covalently

Received: April 9, 2012
Revised: May 24, 2012
Published: May 29, 2012

   dx.doi.org/10.1021/nl301341m | *Nano Lett.* 2012, 12, 3273−3278

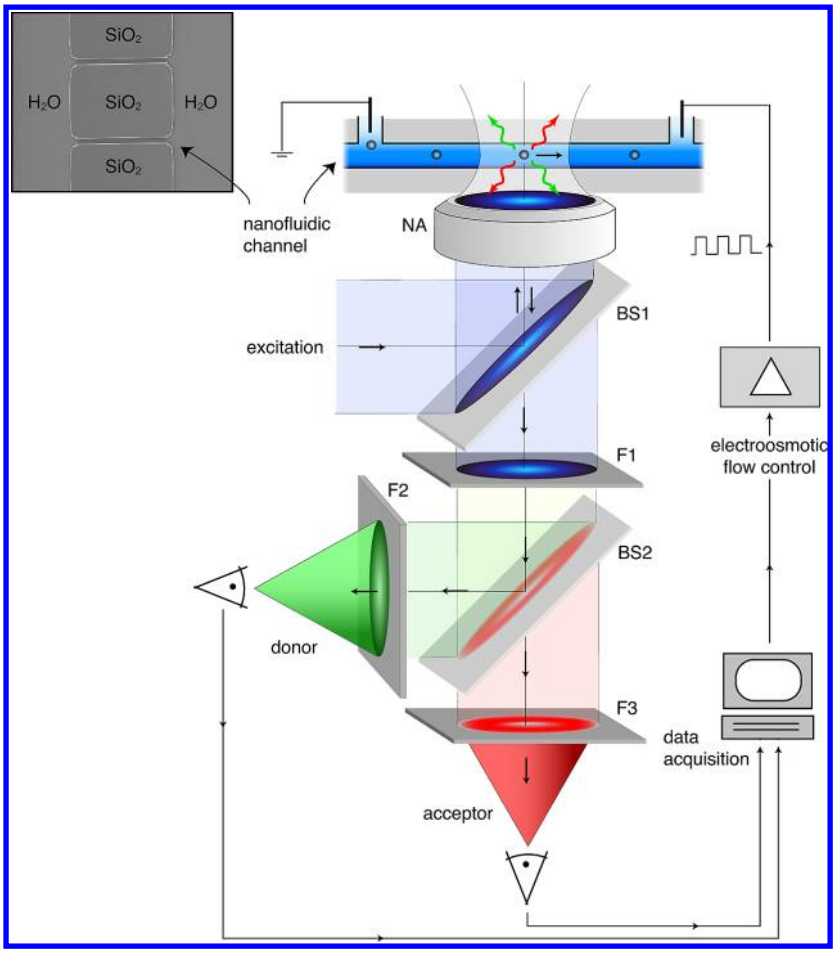

Figure 1. Schematic of single molecule recycling. Donor−acceptor labeled dsDNAs are transported along a nanofluidic channel (cross section ~600 nm × 400 nm) by use of electroosmotic flow. A controller reverses the flow in the nanochannel after detecting a fluorescence burst, causing the molecule to pass through the excitation focus again. This procedure is repeated and makes it possible to sample the same molecule over and over again at periodic times that can be adjusted by the flow speed and the parameters of the flow controller. BS: beam splitter; F: filter; NA: numerical aperture. Inset (top left): SEM image of fabricated nanochannels.

labeled proteins to be confined in liquid environments.[19−21] However, the trapping times are limited by irreversible photobleaching and photoblinking. Since photobleaching increases with laser power and the on and off-times of photoblinking are known to be power-law distributed,[22,23] the total trapping time can only be extended with a sampling protocol that does not require the molecule under investigation to be continuously illuminated. Furthermore, even at low concentrations of molecules there remains a significant probability that two molecules will enter the focus. For reliable detection of single molecules it is critical that a fluorescent detection technique be able distinguish situations in which more than one molecule enters a trap.

The method introduced here is similar to an ABEL trap, but it restricts the motion of a molecule to only one dimension by use of microfabricated nanochannels.[24,25] This configuration allows the trapping of single molecules without the need of continuous observation, which considerably reduces the photobleaching rate and increases the overall trapping time. Furthermore, a one-dimensional scheme is favorable from a device engineering standpoint since it provides a smaller device footprint and easier parallelization, which is of importance for high throughput lab-on-a-chip implementation.

We report here the use of an active approach to extend the total observation duration of untethered single molecules to more than 10 s. The method is based on the use of electroosmosis to drive the transit of a molecule with a constant drift velocity through a laser focused onto a submicrometer channel. After passing through the laser focus, the molecule's direction of motion is reversed, sending it back through the focus. This process can be repeated many hundreds of times for the same dye molecule before photobleaching, or photoblinking occurs or until an "invader" molecule enters the trap. Since we have been able to collect 100−200 photons per pass through the laser focus, as many as tens of thousands photons can be collected from a single fluorescent molecule. The single molecule recycling (SMR) scheme is applicable to various single molecule fluorescence techniques, such as smFRET (single molecule FRET), fluorescence anisotropy, fluctuation analysis for determination of the diffusion constant, or Dexter transfer. Figure 1 illustrates the principle of SMR in the context of smFRET, which is used as a spectroscopic ruler that can monitor nanometer to angstrom scale distance changes between a donor fluorophore and an acceptor fluorophore attached to a single molecule.[26]

The SMR approach has allowed us to perform smFRET measurements of molecules of double-stranded DNA 5′ labeled with Atto 532 and Atto 647N (ATTO-TEC, Germany). The DNA molecules are allowed to traverse the focus of a 532 nm laser focused into a (≈600 nm wide and 400 nm deep)

dx.doi.org/10.1021/nl301341m | *Nano Lett.* 2012, 12, 3273−3278

nanofluidic channel (Supporting Information). A uniform drift velocity of the dsDNA is achieved by applying a voltage across the channel with gold wires dipped into reservoirs as shown schematically in Figure 1. After fluorescence from a dsDNA molecule entering the focus is detected, a countdown timer is started. Following a controllable delay, the potential across the channel is reversed, sending the DNA molecule in the opposite direction back into the laser focus. This process is repeated until eventual photobleaching or photoblinking of the molecule, until an invader molecule enters the SMR, or until the DNA escapes into the reservoir (see Figure 2).

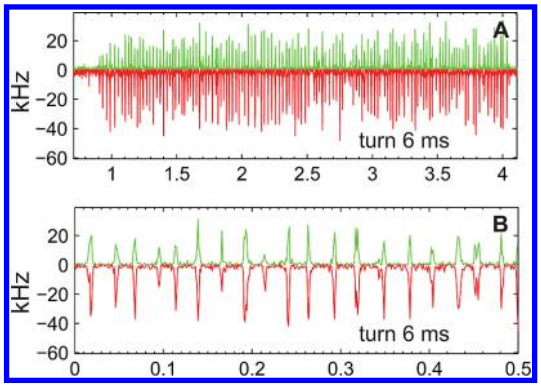

Figure 2. Single molecule recycling of dsDNA13mers. Single dsDNA13mers are captured with the single molecule recycler and measured at the seconds time scale. Donor curves are plotted in green, and acceptor curves are plotted in red. For clarity, acceptor time traces are plotted toward negative values. (A) Recycling of the same dsDNA13mer 144 times in ~3 s with a 6 ms delay in reversal of electroosmosis after the molecule exits the focus. (B) Same data as in panel A, plotted with an expanded time scale demonstrating the optical shutter effect.

Typical fluorescence time courses for SMR of 13 base pair dsDNA molecules are shown in Figure 2. Donor (Atto 532) emission is plotted on the positive *y*-axes (green), and acceptor (Atto 647N) emission is plotted on the negative *y*-axes (red). Panel A shows 144 recycling events over 3 s, achieved using a 6 ms delay between the time the molecule leaves the laser focus and the initiation of field reversal. Panel B shows a portion of the trace in panel A displayed with an expanded time scale. Varying the length of the delay before field reversal makes it possible to collect fluorescence information from the dsDNA over different time intervals.

By adjusting the combination of laser power, focus size, and electrode voltage, it is possible to independently vary the intensity of illumination of the sample and the number of photons collected per recycling event. The photon emission rate can be adjusted by the laser power, whereas the observation time per passage can be controlled by the size of the laser focus and the flow speed. The data shown in Figure 2 used an electroosmotic potential of 80 V, an electrode separation of 1 cm, a laser power of 98 μW, and a laser beam of wavelength λ = 532 nm focused by an objective lens with numerical aperture NA = 1.4. We slightly underfill the back aperture of the objective in order to enlarge the focal spot size; the full NA is used for fluorescence detection. With these settings we obtain roughly 100 photons per passage. The ability to manipulate flow rate and reversal times independently allows the experiment to be conducted over different total time periods, while maintaining useful photon counting statistics.

The motion of molecules undergoing SMR is subject to the relationship between the electroosmotic drift velocity and random Brownian diffusion, as described by the Fokker–Planck equation (Supporting Information).[27,28] Figure 3 shows a

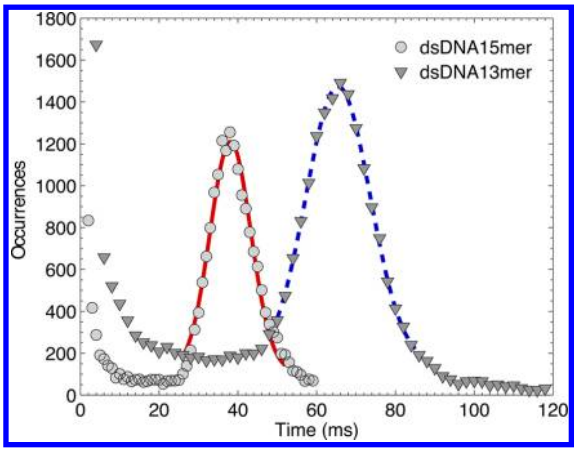

Figure 3. Time between consecutive passes. Distribution of times between one molecule exiting the focus and the next consecutive molecule entering the focus. The peaks at 36.1 ± 0.1 and 65.43 ± 0.06 ms with respective standard deviations 5.2 ± 0.2 and 8.2 ± 0.1 ms correspond to twice the turnaround times of 15 and 30 s plus twice the software loop time ≈2.9 ms for experiments with dsDNA15mers (circles) and dsDNA13mers (triangles), respectively. The widths of the Gaussians are the result of the uncertainty in position due to diffusion. The Gaussians are superimposed on exponential distributions, which describe the times between arrivals of different molecules into the trap.

distribution of the times between one molecule exiting the focus and the next consecutive occurrence of the same molecule entering the focus accompanied by a fit of a Gaussian centered at each peak. For a single molecule that is being recycled, the mean time between exits out of and arrivals into the laser focus is given by twice the turnaround time plus twice the software loop time (the peaks at 36.1 ± 0.1 and 65.43 ± 0.06 ms and with respective standard deviations 5.2 ± 0.2 and 8.2 ± 0.1 ms for the dsDNA15mers and dsDNA13mers, respectively, in Figure 3). The variance of the Gaussian may be used to calculate the diffusion coefficient for one single molecule, $D(x,t)$, whereas typical fluorescence correlation spectroscopy with flow measures the ensemble diffusion properties of molecules.[29] For these measurements, solving for D yields diffusion coefficients of $D \sim (0.98 \pm 0.06) \times 10^{-6}$ cm^2/s for the dsDNA13mer sample and $D \sim (1.3 \pm 0.3) \times 10^{-6}$ cm^2/s for the dsDNA15mer sample. These values are reproduced independently with the diffusion time calculated with the established fluorescence correlation with flow equation (Supporting Information). They are also similar to previous experimentally measured diffusion constants of 1.2×10^{-6} and 1.4×10^{-6} cm^2/s for freely diffusing 14 and 12 bp DNAs, respectively.[30] Differences may be attributable to sequence-specific effects. This provides the potential for discriminating single molecules based on their hydrodynamic radii in addition to their spectroscopic signatures.

In SMR, losses of molecules due to Brownian motion are minimized by the lateral confinement provided by the nanochannels, by using a channel length sufficient to minimize losses to the reservoir, and by using a drift velocity that is larger than the diffusion velocity. Losses of single molecules during

dx.doi.org/10.1021/nl301341m | *Nano Lett.* 2012, 12, 3273–3278

recycling are mainly due to dye photophysics, such as photoblinking and photobleaching. Even when photobleaching is limited, organic dyes have been reported to follow power-law blinking distribution in both their on- and off-times, which we verify for on-time kinetics (Figure S3, Supporting Information).[22]

Photon counting statistics during the short time during which a freely diffusing molecule remains in the laser focus impose a major limitation on the precision of conventional smFRET measurements of diffusing molecules in solution. SMR provides an improvement over free diffusion because the transit time distribution is more uniform and because the introduction of electroosmosis and the control of the size of the focus allows us to collect single pass data with longer times spent inside the laser focus. Figure 4 demonstrates that the

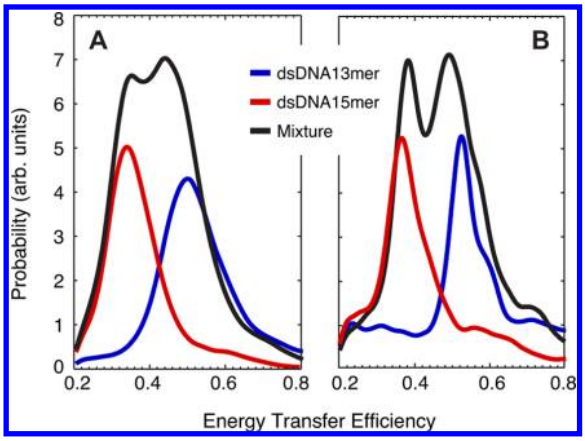

Figure 4. Single molecule recycling combined with spFRET. Distributions of energy transfer efficiency (ETE) for dsDNA molecules of two different lengths (13 and 15 base pairs). Panel B: distributions resulting from measuring different dsDNA only once (standard diffusion-based experiment). 65 030 transits are used for the dsDNA13mer distribution, 120 435 transits for the dsDNA15mer distribution, and 148 830 transits for the mixture. Panel B: Same as in panel A but sampling each dsDNA molecule at least nine times. Single molecule recycling improves the resolution and accuracy. 10 789 transits are used for the dsDNA13mer distribution, 22 875 transits for the dsDNA15mer distribution, and 4341 transits for the mixture. The distribution were created using the function, ksdensity, in MATLAB with a width of (A) 0.015 and (B) 0.02.

resolution in FRET measurements can be enhanced by repeated transits through the focus. In these measurements we have used samples of two different DNA lengths: 13 bp dsDNA, 15 bp dsDNA, and mixtures of the two. Energy transfer efficiency (ETE) values have been calculated by correcting for the finite detection efficiencies and quantum yields of donor and acceptor molecules (ρ = 1.56, Supporting Information). Figure 4A shows a distribution of energy transfer efficiencies for dsDNA molecules that was created from *single passes* through the laser focus, as in traditional solution-based smFRET measurements. A distribution of a mixture of the two dsDNAs is shown in black. The mean energy transfer efficiency for the 13 bp dsDNA is ~0.5, whereas for the 15 bp dsDNA it is ~0.31. The presence of the minor peaks in the distributions could reflect the existence of the donor in two different configurations (consistent with two lifetimes in the absence of the acceptor; cf. Supporting Information). The acceptor (Atto 647N) exhibits only a single-exponential lifetime curve in bulk fluorescence measurements. Figure 4B shows distributions similar to those in Figure 4A but for multiple passages per dsDNA. It is evident that single molecule recycling improves the resolution and the accuracy with which the two different dsDNA lengths can be distinguished. Additional structure in the ETE distributions is evidenced by the non-Gaussian shape of the distributions. A comparison of Figures 4A and 4B shows that the shoulders at high ETE values are preserved, indicating the presence of stable subpopulations of ETE values in samples consisting of one length of dsDNA.

The data presented in Figure 5 demonstrate that it is also possible to employ SMR for single molecule fluorescence

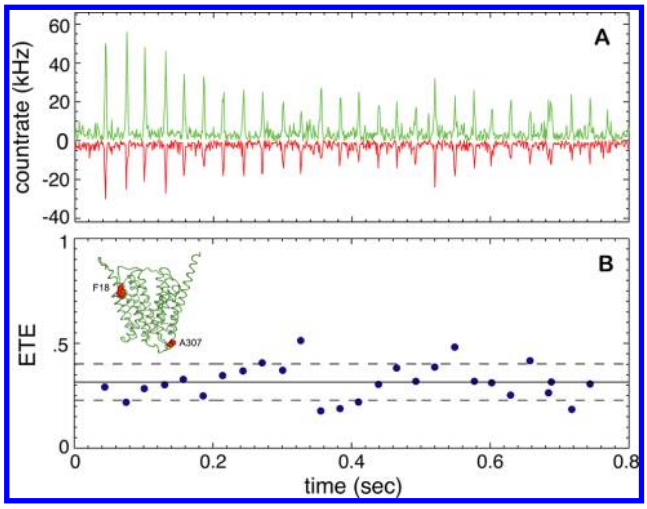

Figure 5. Repeated FRET measurements on a single OxlT membrane protein. Panel A: fluorescence time trace of donor (green) and acceptor (red). Panel B: corresponding energy transfer efficiency (ETE). The mean ETE is 0.315 (solid horizontal line), and the standard deviation is 0.086 (dashed horizontal lines). The variations in ETE are the result of shot noise. The inset shows the homology model of OxlT with the donor and acceptor sites (red features).

measurements on proteins in the presence of surfactants. The trapped molecule in this case is purified oxalate transporter, OxlT, from the bacterium *Oxalobacter formigenes*, a member of the Major Facilitator Superfamily (Law et al., 2008). The experiments were conducted with an allele of OxlT from which the normal two cysteine residues were removed (C28G/C271A) and two cysteine residues were introduced (F18C/A307C). The two introduced cysteines were labeled with Cy3 and Cy5 dyes. OxlT was maintained in the presence of 0.1% (w/v) of the detergent dodecyl-β-D-maltoside and 10 mM potassium oxalate to maintain stability of the protein. The nanochannels were coated with 1 mg/mL poly(L-lysine) to prevent OxlT adsorption to the channel surfaces.

Figure 5A shows a time-trace of donor and acceptor emission of a single OxlT that is being recycled in a nanochannel. The corresponding energy transfer efficiency (ETE) values are plotted in Figure 5B. The mean ETE is 0.315, and the standard deviation is σ = 0.086. These values are indicated in Figure 5B by horizontal lines. Since the variation in ETEs is of the magnitude expected for shot noise, these variations cannot be assigned to changes in the protein structure. These results demonstrate that it is possible to trap single proteins in the presence of detergent and to monitor FRET efficiencies for multiple sequential transits through the focus. Changes in the OxlT structure and the FRET efficiency can be initiated by

dx.doi.org/10.1021/nl301341m | *Nano Lett.* 2012, 12, 3273−3278

changing the substrate conditions (e.g., oxalate or malonate) while a single OxlT protein is being recycled.

Reversible electroosmosis can be used to send individual molecules (DNA, OxlT) back-and-forth through a laser beam focused into a nanofluidic channel. We were able to cycle a single molecule for as long as 15 s, allowing a substantial increase in the precision of smFRET determinations compared with what would be possible by single-pass detection of freely diffusing molecules. Single molecule recycling (SMR) is a "true" single molecule technique, in the sense that it is able to establish a distribution for an individual molecule. This distribution can then be compared with that for other single molecules. This approach is expected to be particularly useful for studying fluctuations and conformational heterogeneity of biomolecules or polymers that may be sensitive to tethering systems and proximity to surfaces. It is also well-suited to examination of proteins in the presence of detergents. It provides the capability to determine precise smFRET efficiencies that can be followed over relatively long time scales relevant to understanding conformational changes underlying protein folding, catalysis, and other biosynthetic and functional mechanisms. Real-time data processing can be implemented to determine the diffusion coefficient of single molecules for potential applications such as DNA sorting. Simultaneous hydrodynamic and smFRET measurements allow diffusion coefficient variations to be correlated with changes in ETE due to conformational changes. The independent measurement of hydrodynamic size in addition to spectral information from different fluorescence channels can increase the number of observable signals in colocalization measurements if different sized molecules are being studied. This technique is also scalable because an array of nanofluidic channels on the same microfluidic device can be used to track many molecules at the same time. The illumination could come from multiple confocal spots focused in different nanochannels or from a line focused by a cylindrical lens across the nanochannel array. The flexibility of this approach will also allow it to be integrated into present and future microfluidic or nanofluidic devices.

■ ASSOCIATED CONTENT

Supporting Information

Fluorescent labeling of OxlT proteins; single molecule FRET, lifetime, and diffusion measurements; data acquisition and measurement techniques; and fabrication of nanofluidic channels. This material is available free of charge via the Internet at http://pubs.acs.org.

■ AUTHOR INFORMATION

Corresponding Author

*E-mail: lukas.novotny@rochester.edu.

Notes

The authors declare no competing financial interest.

■ ACKNOWLEDGMENTS

We thank Zachary J. Lapin for help with editing the manuscript and Zhenzhen Jia and Di-Cody Kang for providing purified OxlT mutants. This work was supported in part by NIH (Grants 1R21AI085543-01A1 and GM24195) and by a Provost's Multidisciplinary Award by the University of Rochester. The nanochannels were fabricated at the Cornell NanoScale Facility, a member of the National Nanotechnology Infrastructure Network, which is supported by NSF (Grant ECS-0335765).

■ REFERENCES

(1) Zhuang, X.; Ha, T.; Kim, H. D.; Centner, T.; Labeit, S.; Chu, S. Fluorescence quenching: A tool for single-molecule protein-folding study. *Proc. Natl. Acad. Sci. U. S. A.* **2000**, *97*, 14241−14244.

(2) Weiss, S. Fluorescence spectroscopy of single biomolecules. *Science* **1999**, *283*, 1676−1683.

(3) Brunger, A.; Weninger, K.; Bowen, M.; Chu, S. Single molecule studies of the neuronal SNARE fusion machinery. *Annu. Rev. Biochem.* **2009**, *78*, 903−928.

(4) Roy, R.; Kozlov, A.; Lohman, T.; Ha, T. SSB protein diffusion on single-stranded DNA stimulates RecA filament formation. *Nature* **2009**, *461*, 1092.

(5) Tsai, W. H.; Tsao, Y. C.; Lin, H. Y.; Shen, B. C. Cross-point analysis for a multimode fiber sensor based on surface plasmon resonance. *Opt. Lett.* **2005**, *30*, 2209−2211.

(6) Adachi, K.; Yasuda, R.; Noji, H.; Itoh, H.; Harada, Y.; Yoshida, M.; Kinosita, K., Jr. Stepping rotation of F1-ATPase visualized through angle-resolved single-fluorophore imaging. *Proc. Natl. Acad. Sci. U. S. A.* **2000**, *97*, 7243−7247.

(7) Pal, P.; Lesoine, J. F.; Lieb, M. A.; Novotny, L.; Knauf, P. A. A novel immobilization method for single protein spFRET studies. *Biophys. J.* **2005**, *89*, L11−L13.

(8) Huang, J.; Nagy, S.; Koide, A.; Rock, R. A Peptide Tag System for Facile Purification and Single-Molecule Immobilization. *Biochemistry* **2009**, *48*, 11834.

(9) Chung, H.; Louis, J.; Eaton, W. Distinguishing between protein dynamics and dye photophysics in single-molecule FRET experiments. *Biophys. J.* **2010**, *98*, 696.

(10) Gansen, A.; Valeri, A.; Hauger, F.; Felekyan, S.; Kalinin, S.; Toth, K.; Langowski, J.; Seidel, C. Nucleosome disassembly intermediates characterized by single-molecule FRE. *Proc. Natl. Acad. Sci. U. S. A.* **2009**, *106*, 15309.

(11) Goldsmith, R. H.; Moerner, W. Watching conformational- and photodynamics of single fluorescent proteins in solution. *Nat. Chem.* **2010**, *2*, 179−186.

(12) Nir, E.; Michalet, X.; Hamadani, K. M.; Laurence, T. A.; Neuhauser, D.; Kovchegov, Y.; Weiss, S. Shot-noise limited single-molecule FRET histograms: comparison between theory and experiments. *J. Phys. Chem. B* **2006**, *110*, 22103−22124.

(13) Werner, J. H.; McCarney, E. R.; Keller, R. A.; Plaxco, K. W.; Goodwin, P. M. Increasing theresolution of single pair fluorescence resonance energy transfer measurements in solution via molecular cytometry. *Anal. Chem.* **2007**, *79*, 3509−3513.

(14) Hamadani, K.; Weiss, S. Nonequilibrium single molecule protein folding in a coaxial mixer. *Biophys. J.* **2008**, *95*, 352.

(15) Vogelsang, J.; Doose, S.; Sauer, M.; Tinnefeld, P. Single-molecule fluorescence resonance energy transfer in nanopipets: Improving distance resolution and concentration range. *Anal. Chem.* **2007**, *79*, 7367−7375.

(16) Boukobza, E.; Sonnenfeld, A.; Haran, G. Immobilization in surface-tethered lipid vesicles as a new tool for single biomolecule spectroscopy. *J. Phys. Chem. B* **2001**, *105*, 12165−12170.

(17) Diao, J.; Yoon, T.; Su, Z.; Shin, Y.; Ha, T. C2AB: A Molecular glue for lipid vesicles with a negatively charged surface. *Langmuir* **2009**, *25*, 7177−7180.

(18) Okumus, B.; Wilson, T. J.; Lilley, D. M. J.; Ha, T. Vesicle Encapsulation studies rReveal that single molecule Ribozyme heterogeneities are intrinsic. *Biophys. J.* **2004**, *87*, 2798−2806.

(19) Cohen, A. E.; Moerner, W. E. A method for trapping and manipulating nanoscale objects in solution. *Appl. Phys. Lett.* **2005**, *86*, 093109.

(20) Cohen, A. E.; Moerner, W. E. Controlling Brownian motion of single protein molecules and single fluorophores in aqueous buffer. *Opt. Express* **2008**, *16*, 6941−6956.

(21) Fields, A. P.; Cohen, A. E. Electrokinetic trapping at the one nanometer limit. *Proc. Natl. Acad. Sci. U. S. A.* **2011**, *108*, 8937−8942.

(22) Hoogenboom, J. P.; Hernando, J.; van Dijk, E. M. H. P.; van Hulst, N. F.; Garcia-Parajo, M. F. Power-law blinking in the fluorescence of single organic molecules. *ChemPhysChem* **2007**, *8*, 823−833.
(23) Cichosa, F.; Borczyskowskib, C.; Orrit, M. Power-law intermittency of single emitters. *Curr. Opin. Colloid Interface Sci.* **2007**, *12*, 272−284.
(24) Gershow, M. C.; Golovchenko, J. A. Recapturing and trapping singlemolecules with a solid-state nanopore. *Nat. Nanotechnol.* **2007**, *2*, 775−779.
(25) Mitra, A.; Deutsch, B.; Ignatovich, F.; Dykes, C.; Novotny, L. Nano-optofluidic detection of single viruses and nanoparticles. *ACS Nano* **2010**, *4*, 1305−1312.
(26) Roy, R.; Hohng, S.; Ha, T. A practical guide to single-molecule FRE. *Nat. Methods* **2008**, *5*, 507−516.
(27) Fokker, A. D. Die mittlere Energie rotierender elektrischer Dipole im Strahlungsfeld. *Ann. Phys.* **1914**, *43*, 810−820.
(28) Planck, M. Über einen Satz der statistichen Dynamik und eine Erweiterung in der Quantumtheorie. *Sitzungber. Preuss. Akad. Wiss.* **1917**, 324−341.
(29) Kohler, R. H.; Schwille, P.; Webb, W. W.; Hanson, M. R. Active protein transport through plastid tubules: velocity quantified by fluorescence correlation spectroscopy. *J. Cell Sci.* **2000**, *113*, 3921−3930.
(30) Fernandes, M. X.; Ortega, A.; Martinez, M. C. L.; de la Torre, J. G. Calculation of hydrodynamic properties of small nucleic acids from their atomic structure. *Nucleic Acids Res.* **2002**, *30*, 1782.

Nanochannel Based Single Molecule Recycling

John F. Lesoine,[†] Prahnesh A. Venkataraman,[‡] Peter C. Maloney,[¶] Mark Dumont,[‡] and Lukas Novotny[*,†]

Institute of Optics, University of Rochester, Department of Biochemistry and Biophysics, University of Rochester, and Department of Physiology, Johns Hopkins University

E-mail: lukas.novotny@rochester.edu

Supporting Information Available

Fluorescent labeling of OxlT

Purified double cysteine mutant F18C-A307C was exchanged into buffer containing 50 mM Tris-Cl pH 7.5, 10 mM Oxalate, 20% glycerol by two passages through Microbio-spin P30 spin columns (Biorad) equilibrated with the same buffer. 10 μM protein (cysteine:total dye ratio of 1:2) was mixed with 33.3 μM of Cy5-MTSEA and 6.7 μM Cy3-MTSEA (Toronto Research Chemicals) and incubated on ice for 30 minutes. Unreacted dye was removed by two passages through the same spin columns. The sample was then filtered through a 0.22 μm centrifugation filter to remove any large aggregates. For observation of OxlT in nanochannels, the buffer solution was supplemented with 2 mM 6-Hydroxy-2,5,7,8-tetramethylchromane-2-carboxylic acid (Trolox), 2 mM nitrobenzyl alcohol, 50 nM protocatechuate-3,4-dioxygenase, 2 mM protocatechuic acid (PCA/PCD oxygen scavenging system), and 1 mg/ml poly-L-lysine. The non specific labeling (determined by

[†]Institute of Optics, University of Rochester, Rochester NY 14627
[‡]Department of Biochemistry and Biophysics, University of Rochester Medical Center, Rochester, NY 14627
[¶]Department of Physiology, Johns Hopkins Medical School, Baltimore, MD, USA

comparison to a cys-less form of the protein) was less than 4%. The labeling efficiency at the dye concentration used was approximately 60%, based on measurement of the absorbances of the labeling dyes.

Single molecule FRET measurements

Donor and acceptor bursts were corrected for background and cross-talk using the equations for smFRET

$$A = n_A - BG_A - \chi_{DA}(n_D - BG_D) - \chi_{A0}D^0, \quad (1)$$

$$D = n_D - BG_D - \chi_{AD}(n_A - BG_A); \quad (2)$$

where n_A and n_D are the number of photons in the acceptor or donor channel, and BG_A and BG_D are the acceptor and donor backgrounds. χ_{DA} is the cross-talk of the donor into the acceptor channel, χ_{AD} is the cross-talk of the acceptor into the donor channel, and $\chi_{A0}D^0$ is the direct excitation of the acceptor. χ_{AD} and $\chi_{A0}D^0$ are negligible and therefore set to zero. The relative energy transfer efficiency is then calculated from the ratio of A to $A+D$ with the equation

$$ETE = \frac{A}{A+\rho D}, \quad (3)$$

where $\rho = \frac{\eta_A \phi_A}{\eta_D \phi_D}$ is the ratio of the detection efficiencies of the acceptor to the donor detection channels, $\frac{\eta_A}{\eta_D}$, multiplied by the ratio of the quantum yields of the acceptor to the donor dyes $\frac{\phi_A}{\phi_D}$. The variable, ρ, is required to perform accurate ETE measurements. This allows ETE values to be converted into relative distance values through the relationship

$$ETE = \frac{1}{1+x^6}, \quad (4)$$

where x is the donor-acceptor distance. Changing values of ρ would slightly stretch the resulting ETE histograms because the calculation of ETE values has a nonlinear relationship between A and D.

Single molecule measurements were performed with a circularly polarized 532 nm Nd:YAG laser that passed through a 532/10nm filter and then reflected off of a dichroic beamsplitter (532DCXR; Chroma, VT) and projected on the back aperture of a Nikon NA 1.4 Plan-Apo 60× oil immersion objective. The beam underfilled the back aperture to control the size of the focus in the channel. Fluorescence is collected with the same microscope objective. The collected photons are passed through a dichroic beamsplitter and a longpass filter (540LP; Chroma, VT) to suppress photons from the excitation beam. A dichroic filter (645DCXR; Chroma, VT) is used to separate donor emission from acceptor emission, as illustrated in Figure 1. The acceptor emission is passed through a 690/75nm bandpass filter and the donor emission through a 555/25nm bandpass filter. Single photon detection was achieved using avalanche photo-diodes (SPCM-AQR-14; Perkin Elmer, MA). TTL pulses from the photo-diodes were detected with a LabView 6602 counter card. Time series data were recorded with a custom written LabView software and were analyzed in MATLAB.

Data acquisition

Fluorescence bursts were identified with a burst search algorithm for constant time-binned data.[1] This method is based on establishment of two thresholds where one is the minimum number of photons for a single bin and the other is the threshold for the total number of photons in consecutive bins above the initial threshold. The background count rate is the count rate when a fluorescent molecule is not present in the laser focus. The donor and the acceptor background count rates were 600 Hz and 800 Hz respectively. The data was binned to 1 ms. The first of these thresholds was set at the combined background count for 1 ms plus 4 times the square root of the background

counts for 1 ms or 7 counts rounding up. This threshold was chosen to limit the number of false positive detection events in the time-binned data. The background counts are modeled by Poisson counting statistics and the square root of the average count rate is the standard deviation. Each data set was manually fitted in MATLAB to determine the background count rate and to verify that the background is modeled by Poisson statistics. Setting the threshold to these values and using Poisson counting statistics predicts a false positive detection rate due to shot noise of 0.006%. This would result in approximately 1000 false positive detection events for the data that was collected for 60 minutes with 200 μs time-bins. This does not take into account false positives from possible auto-fluorescent molecules.

The second threshold was set to 40 photons to further reduce false positive detection events and to provide sufficient photons for a precise ETE measurement. With a dedicated time-tagged single photon counting device, the bursts could be identified using the photon arrival times.[2] Once bursts were detected this was sufficient to establish the exact timing of the entrances into and out of the laser focus. Recycling events were discriminated by selecting consecutive bursts spaced within the time window allowed by recycling and diffusion. Thus, if there is an average spacing of 65 ms between events, then the bursts must demonstrate this average spacing with an uncertainty determined by the diffusion coefficient and the elapsed time according to Equation 5 (Supporting Information). The time resolution of the feedback is currently limited by the 2 ms loop time in LabView. Faster time resolution could be achieved with real-time LabView hardware or a dedicated FPGA that is programmed to detect single molecule bursts by analyzing photon arrival times in real-time. The photon counting data is independently recorded with 200 μs time resolution. Any time resolution may be used to record the photons including recording the individual photon arrival times. The 200 μs time was chosen here because it allowed multiple samples on average to be collected as a biomolecule was transiting through the laser focus while allowing manageable file sizes for data that could be recorded for up to three hours.

Expression and Purification of OxlT

A mutant form of OxlT containing two cysteine substitutions (F18C-A307C) was generated by QuikChange site-directed mutagenesis of plasmid using the cysteine-less variant (C28G, C271A) carrying a C-terminal His10 tag as a template.[3,4] Expression and purification of the mutant OxlT were carried out essentially as described previously.[5] In brief, a single colony of Escherichia coli strain XL3 was grown overnight at 37° C in LB medium. This preculture was diluted 100-fold into fresh LB medium and cultured at 35° C to an A650 of 0.1. Expression was induced by addition of 1 mM isopropyl-1-thio-β–D-galactopyranoside, followed by an additional 3 h of growth. Harvested cell pellets were lysed by sonication for 10 min (5 sec on, and 5 sec off) at 4° C, at power level 5 with Ultrasonic XL2020 sonicator (Misonix, NY) in a buffer (pH 7.5) containing 20% (v/v) glycerol, 200 mM potassium oxalate, 50 mM Tris-HCl, and 1 mM phenylmethanesulfonylfluoride. Membrane proteins solubilization was performed with 1% (w/v) β-dodecylmaltoside (DDM) (Anatrace, OH) at 4° C for 1 h. The insoluble material was removed by ultracentrifugation (324,000 g x 30 min). The supernatant was then incubated with Ni-NTA resin (Qiagen, CA) at 4° C for 4 h followed by washing with 100 bed volumes of buffer containing 20% glycerol, 200 mM potassium oxalate, 20 mM Tris-HCl (pH 7.5), 40 mM imidazole, and 0.1% DDM. OxlT was eluted using a buffer containing 20% glycerol, 200 mM potassium oxalate (pH 4.3), 50 mM acetic acid, 10 mM TCEP, and 0.1% DDM. The protein was then concentrated using an Amicon concentrator with 30 KDa MWCO.

Nucleic acid sample preparation

Nucleic acid sequences were selected so that the most stable secondary structure is the properly aligned heterodimer of each single stranded nucleic acid sequence with its complement. Sequences of different lengths were designed so that they do not interact favorably with one another. Nucleic acids terminally labeled with Atto 532 and Atto 647N were purchased from Atto-Tec, Germany. The nucleic acids were 5 prime labeled with either ATTO 532 or ATTO 647N by coupling the NHS

esters of the dyes to a 5'-C6-amino linker of the oligos.

The dsDNA 13mer sequences used were 5' Atto 532 - CGC ATG CAG GCT G 3' and 5' Atto 647N - CAG CCT GCA TGC G 3'. The dsDNA15mer sequences were 5' Atto 532 - GCA CTC AGA GGA CCG 3' and 5' Atto 647N - CGG TCC TCT GAG TGC 3'. The single stranded nucleic acids were annealed with a 2:1 stoichiometric ratio of Atto 647N labeled strands to Atto 532 labeled strands in 40mM Tris-Acetic acid pH 8.3 buffer with 50mM NaCl. The samples were heated to 90°C in a metal heat block and then the block was removed from the hot plate and the samples were allowed to cool to 30°C in the block before being stored on ice. After annealing, aliquots of dsDNA were frozen at -20°C. Atto 532 and Atto 647N were chosen because of their resistance to photobleaching and their high quantum yields.

Single molecule measurements were performed in 40 mM Tris-Acetic acid buffer at pH 8.3 with 10mM NaCl and 2mM $MgCl_2$ to increase the melting temperature of the dsDNA. The experiments were performed at room temperature which was 20°C. The buffer also contained 30% v/v glycerol to prevent evaporation, 0.5% Tween- 20 to prevent nonspecific adsorption of the nucleic acids to the channel surface, and anti-oxidants to prevent photophysical artifacts:[6] 2mM Trolox (Sigma-Aldrich, St. Louis, MO), 2mM Nitro Benzyl Alcohol (Sigma-Aldrich, St. Louis, MO), and the protocatechuic acid (PCA)/protocatechuate-3,4-dioxygenase (PCD) (Sigma-Aldrich, St. Louis, MO) oxygen scavenging system with 2mM PCA and 50nM PCD.[7]

Fabrication of Nanofluidic Channels

Double-side-polished (DSP) fused silica wafers (100 mm diameter, 300 μm thick, surface roughness $< 0.5\,\mathrm{nm_{rms}}$) from Mark Optics were RCA1 (HCL:H2O2:H2O) cleaned for 20 min at 70°C right out of the box. Following that, the wafers were vapor-primed at 150°C (YES LP-III Vapor Prime Oven, HMDS) and spin-coated with OiR 620-7i photoresist (3000 rpm, 30 sec, 600 nm).

After soft-baking the resist (90°C, 60 sec), subsequent exposure was accomplished using both optical and contact lithography. The smaller, nm-sized features were exposed using a GCA-6300 10x i-line Stepper (General Signal Corp, Andover, MA, 1.4 sec exposure) and the larger um-sized features were exposed using an EV-620 Contact Aligner (Electronic Visions, Phoenix, AZ, 5 sec exposure). Resist development using MIF300 (60 sec, Single Puddle) in the Hamatech/Steag wafer developer followed each of the exposures. After final development, the fused silica wafers were hardbaked (BLE Hotplate, 115°C, 120 sec) to drive off solvents and densify the remaining resist film. Also, a brief oxygen plasma de-scum (Glenn 1000, 100 watts, Shelf b, 60 sec) was performed to clear any unwanted resist prior to reactive ion etching (RIE). The nanofluidic channels were etched into the exposed surface of the fused silica wafers using CHF3O2 etch chemistry in an Oxford 80 RIE (50 sccm CHF3, 2 sccm O2, 240 watts RF, 40 mTorr, 12°C) for 35 minutes. Sealing of the nanofluidic channels was accomplished by wafer direct bonding (WDB) of a second un-etched fused silica wafer with through holes, for reservoirs, onto the first.[8] After spinning a protective resist layer (Shipley S1827, 3000 rpm, 45 sec) on both sides of the top wafer and labeling the holes to be drilled with an indelible marker, reservoir access through holes were drilled into the top wafer using an AirBrasive 6500 System2 sand blaster tool (using 50 μm aluminum oxide powder from SS White Technologies, Piscataway, NJ). After drilling the top wafer, each pair of wafers to be bonded (i.e. the top and bottom wafers) were subjected to a thorough cleaning regimen that included: (1) an acetone bath with DI water rinse, (2) a second acetone bath with DI water rinse, (3) a hot strip bath (propylene-glycol, n-methyl-pyrrolidone, tetra-methylammonium- hydroxide, 20 min at 75°C), (4) a detergent/water bath with sonication and DI water rinse, (5) a methanol bath (5 min) with DI water rinse, (6) an acetone bath (5 min) with DI Water rinse, (7) a hot nanostrip bath (H2SO4:H2O2, 2 hrs at 50°C) with x3 DI water rinses and (8) an RCA1 clean with x3 DI water rinses. After the final RCA1 clean and rinse, the wafers were kept in DI water until they were ready for bonding. Underwater, room-temperature bonding was performed by removing one top wafer (with the access holes) and one bottom wafer (with the etched nanofluidic channels), aligning their major/minor flats and pressing them firmly together underwater for a period of nominally

30 sec. Then, they were removed and allowed to dry (horizontally) for a period of 3 hours and dried (horizontally) in a convection oven (90°C, 12 hrs). A final furnace anneal (1050°C, 30 min) caused the weaker Van der Waals and/or hydrogen bonds to be replaced by considerably stronger covalent bonds. Images of 15 μm long channels are provided in Figure S1.

Surface Passivation in the Nanochannels

A stable coating may be required for some biological molecules to prevent nonspecific adsorption to the fused silica surfaces inside of the channels. Tween-20 at 0.5% v/v is present in the nucleic acid samples to prevent interactions with the surfaces. Poly-l-lysine at 1 mg/mL is present in the OxlT buffer to prevent nonspecific adsorption of the positively charged OxlT to the glass substrate. First 2 μL of the respective buffer is added to one the reservoirs. After the channel is filled another 2 μL is added to the other reservoir. This is allowed to sit for at least 10 minutes while the background signal is collected. The biomolecules are then diluted in their respective buffers. The buffer is removed from each reservoir and then the diluted sample is added to each reservoir.

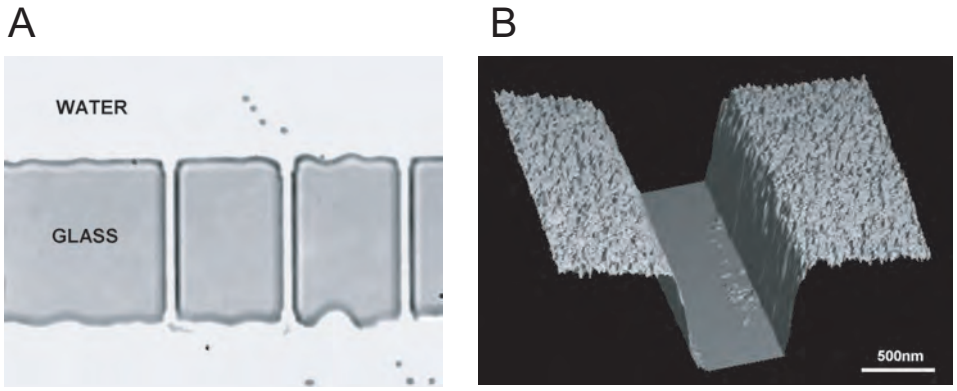

Figure 1: **Characterization of Fabricated Nanochannels**. A: Optical image of 15 μm long nanochannels fabricated into a glass barrier that divides a larger microfluidic channel. B: AFM image of the cross-section of a single nanochannel.

Measuring Diffusion with Single Molecule Recycling

The motion of molecules undergoing SMR is subject to the relationship between the electroosmotic drift velocity and random Brownian diffusion, as described by the the Fokker-Planck equation,[9,10]

$$\frac{\partial}{\partial t}p(x,t) = -\frac{\partial}{\partial x}[v(x,t)p(x,t)] + \frac{\partial^2}{\partial x^2}[D(x,t)p(x,t)]\,, \tag{5}$$

where $p(x,t)$, gives the probability of finding the particle at time t at position x. $D(x,t)$ is the diffusion coefficient and $v(x,t)$ is the velocity. The latter represents the terminal velocity defined by electroosmosis, electrophoresis and the viscosity, η. The solution to this equation in one dimension with a constant drift velocity is:

$$p\,(x,t) = \frac{1}{\sqrt{4\pi Dt}}\exp\left(-\frac{(x-vt)^2}{4Dt}\right)\,, \tag{6}$$

where $D(x,t)$ is assumed to be a constant. $p\,(x,t)$ represents a Gaussian amplitude function, the variance of which ($\sigma^2 = 2Dt$) scales linearly with t and D. If $t = 0$ is defined as the time when the particle is in the center of the laser focus, then the uncertainty in the position increases with time as the particle exits the focus. The distribution's center is determined by the summation of the different flow velocities (for these measurements one speed and two directions) multiplied by the elapsed time.

Figure 3 in the main text shows a histogram of the times between one dsDNA molecule exiting the focus and the next consecutive occurrence of a dsDNA molecule entering the focus. The data is accompanied by a fit of a Gaussian plus an exponential. For one molecule that is being recycled, the mean time between exits out of and arrivals into the laser focus is given by twice the turnaround time plus twice the software loop time (peak at 65 ms). The variance in the time between recycling events multiplied by the squared mean velocity of the particle is approximately equal to the variance of Equation 5, i.e. $\sigma^2 = 2Dt$. The velocity can be calculated with the mean transit times and the size of the Gaussian focal spot or from the autocorrelation of the fluorescence

signal using the fluorescence correlation spectroscopy equation with a flow slightly modified for the dimensions of the nanochannels,[11]

$$G(\tau) = \frac{G(0)\exp\left[-\frac{(\tau/\tau_v)^2}{1+\tau/\tau_D}\right]}{\left[1+\frac{\tau}{\tau_D}\right]^{1/2}\left[1+\left(\frac{\omega_x}{\omega_y}\right)^2\frac{\tau}{\tau_D}\right]^{1/2}\left[1+\left(\frac{\omega_x}{\omega_z}\right)^2\frac{\tau}{\tau_D}\right]^{1/2}} + G(\infty). \quad (7)$$

Here $G(\tau)$ is the correlation function with τ (the correlation time) as the independent variable. τ_D is the mean diffusion time in the x-direction along the direction of flow, τ_v is the transit time through the focus along the direction of flow without diffusion, $G(0)$ is the y-intercept, $G(\infty)$ is the steady state value of the correlation function, ω_x is the distance of the focus along the direction of the channel, ω_y is the width of the channel and ω_z is the height of the channel. In our experiments the width of the channels, ω_y, was 650 ± 50 nm, the height of the channels, ω_z, was 450 ± 20 nm, and the width of the focus, ω_x, was 960 ± 60 nm. For the dsDNA13mer $\tau_D = .0125 \pm .0003s$, $\tau_v = 0.00337 \pm .00002s$ and $G(0) = 0.421 \pm 0.002$. For the dsDNA15mer $\tau_D = 0.0074 \pm .0004s$, $\tau_v = 0.00188 \pm .00002s$ and $G(0) = 0.399 \pm 0.004$. These times are with respect to transiting the direction of flow defined as the x-direction. Diffusion coefficients were also calculated based on the τ_D values for the dsDNA13mer and dsDNA15mer and they were not statistically different from the values calculated based on variance in times between arrivals of the same molecule into the focus. This is easily performed by taking 960 nm squared and dividing by the τ_D values. The errors are quoted as standard deviation values. In the linear regime, flow speed scales with the applied electric field. The flow speed for the dsDNA15mer, for 150 V, is predicted to be 1.66 times faster than for the flow speed of the dsDNA13mer at 90 V. The actual ratio is $1.79 \pm .09$ and this is in statistical agreement with the 1.66 value as predicted by simple linear electroosmotic theory.

It is also interesting to note the peaks in the autocorrelation function in Figure S2 at times corresponding to the periods of the recycling events. The widths of these revival peaks are a reflec-

tion of the variance in position due to diffusion. The peaks can be seen to decrease in amplitude, which is in part due to the increase in position uncertainty spreading in time from the first recycling event. As the width of the peaks increase the amplitudes will decrease to conserve the area under the autocorrelation function. The effect of SMR is to reset this uncertainty each time the molecule passes through the laser focus. This deterministic behavior also allows us to continue to recycle molecules that blink, although, in this case, the uncertainty will not be reset after each pass through the focus so the probability of losing the "dark" molecules increases with time until the molecule switches on or is lost from the trap.

The experimental dsDNA diffusion coefficient that was measured in the nanochannels agrees well with the diffusion coefficient measured in bulk measurements. Diffusion in channels can also be influenced by the close proximity to surfaces or the transient nonspecific adsorption to surfaces.[12] Thus the channel geometry and the surface passivation strategy can also impact the diffusion coefficient measured in nanochannels. In these pseudo-1-dimensional diffusion experiments the variable diffusion along the nanoscale dimensions did not produce an experimental diffusion coefficient in the direction of flow that was statistically different from bulk measurements. This is

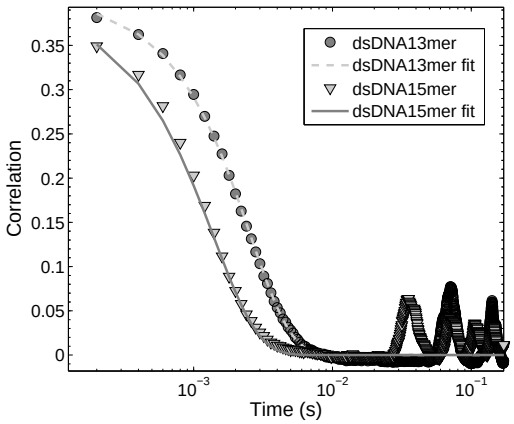

Figure 2: **Fluorescence autocorrelation of labeled dsDNA with flow in nanochannels.** The autocorrelation curve is a function of both the flow speed as well as free diffusion of dsDNA molecules. The curves are fits according to $G(\tau)$. The peaks in the autocorrelations at longer times are due to repeated recycling of single molecules.

confirmed experimentally with both FCS and by the standard deviation method developed in this manuscript.

Loss of Particles from the Trap

In SMR, losses of molecules due to Brownian motion are minimized by the lateral confinement provided by the nanochannels and by using a drift velocity that is larger than the diffusion velocity. In addition, the use of sufficiently long nanochannels (15 to 50 μm) prevents the loss of molecules during reversal of the applied potential. Losses of single molecules during recycling are, thus, mainly due to dye photophysics, such as photoblinking or photobleaching. The dye photophysics determines the shape of the distribution of the histogram of the number of recycling events for each single molecule, since there is constant excitation from the laser beam and relatively constant photon emission from repeated transits due to the constant velocity imposed by electroosmosis and the confinement in the nanochannels. The distribution of the on-times, or similarly the total number of photons before blinking, is therefore directly responsible for shaping the distribution of trapping times. Even when photobleaching is limited, organic dyes have been reported to follow power-law blinking distribution in both their on- and off-times.[13] Figure S3 (A) shows a histogram of the behavior for the total number of photons collected for each single dsDNA13mer molecule before it was lost from the trap in a three hour run. The arrow 1 points to photon numbers that correspond to the numbers found from a single pass through the laser. The arrow 2 corresponds to photon numbers that account for more than one pass through the laser focus before loss from the trap. Figure S3 (B) shows the influence of dye photophysics on the total number of recycling events.

To help follow a molecule after a blinking event we implemented an algorithm that initiates a flow reversal even if that molecule transits through the laser focus and does not emit a fluorescence burst. Thus, SMR can prolong transits by making use of information given by the drift velocity

and the periodicity of detection events. At useful concentrations of labeled target molecules in solution. There is a finite probability that a second “invader” molecule will enter the nanochannel while one molecule is undergoing recycling. While low molecule concentrations greatly reduce the risk of such events, the number of molecules in the trap can be extracted from the timing sequence of detection events as deviations from the expected behavior of single molecules according to the flow and diffusion dynamics described by Equation 6 and hence, it is always possible to verify that only a single molecule is being recycled. This is easily seen by examination of the timing of photon bursts shown in Figure S4. When two molecules enter at the same time, they will eventually diffuse apart and this will be evident in the timing of the transits through the channel. Similar features of the timing of photon bursts will also allow detection of a situation in which an "invader" molecule enters a channel in which a previously-trapped molecule is undergoing transits.

Fluorescence lifetime measurements

Both fluorescence lifetime and steady state fluorescence intensity measurements were performed for purposes of comparison with single molecule studies. Fluorescence lifetime measurements

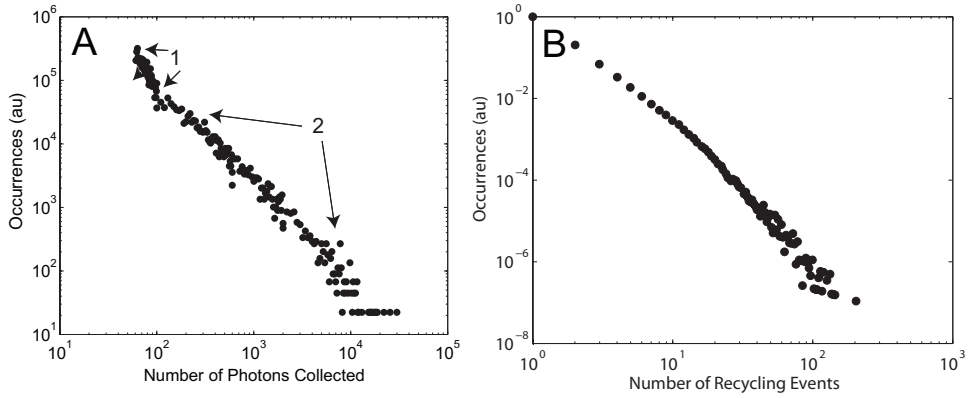

Figure 3: **Histograms revealing a power-law behavior for the total number of photons and transits for SMR.** A: A log-log plot showing a histogram of the total number of photons collected for each recycled molecule. The histogram has been recorded for a solution of dsDNA13mers over a time of 3 hours. B: The histogram of the number of transits through the laser focus for each SMR molecule for the same data.

were conducted using a Fluoromax-4 instrument from HoribaJobin Yvon equipped with a TCSPC module. The Atto 532 donor was excited with a 462 nm NanoLED using a 457 nm/30 nm bandpass filter. Direct emission from donor was detected at 533 nm using a 500 nm long-pass filter. Where indicated, direct excitation of the Atto 647N acceptor was accomplished using a 625 nm NanoLED with a 625 nm/15 nm bandpass filter. Acceptor emission was detected at 705 nm using a 700 nm long-pass filter. Fitting of fluorescence lifetimes was accomplished using the DAS6 software provided with the instrument. Ludox (Sigma Aldrich) colloidal silica particles were used as scatterers to monitor the instrument response (prompt).

ETE was calculated from fluorescence lifetime data by comparing the lifetimes of the donor in the absence of the acceptor to the lifetimes in the presence of acceptor. The lifetime of the donor in the presence of the acceptor is related to the lifetime of the donor in the absence of the acceptor and to the rate of energy transfer

$$ETE = 1 - \frac{\tau_{DA}}{\tau_D}. \tag{8}$$

where τ_D is the lifetime of the donor in the absence of the acceptor, τ_{DA} is the lifetime of the donor in the presence of the acceptor and ETE is the energy transfer efficiency.

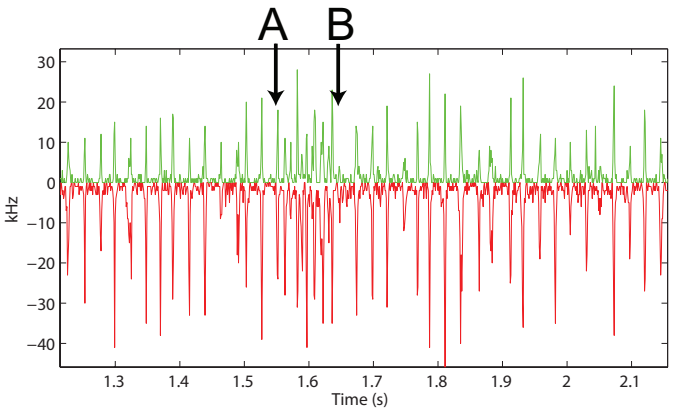

Figure 4: **Identification of "invader" molecules in SMR.** SMR occurs until the time marked by the arrow A when an "invader" molecule enters the trap. Two molecules are undergoing recycling until one of them leaves at the time marked by the arrow B, after which SMR of the surviving molecule resumes.

Fluorescence decays and the corresponding exponential fits for the decays of fluorescence of Atto 532 attached to dsDNA13mers and 15mers in the presence and in the absence of Atto 647N are plotted in Figure S3. The lifetime data extracted from fitting of the decay curves in Figure S3

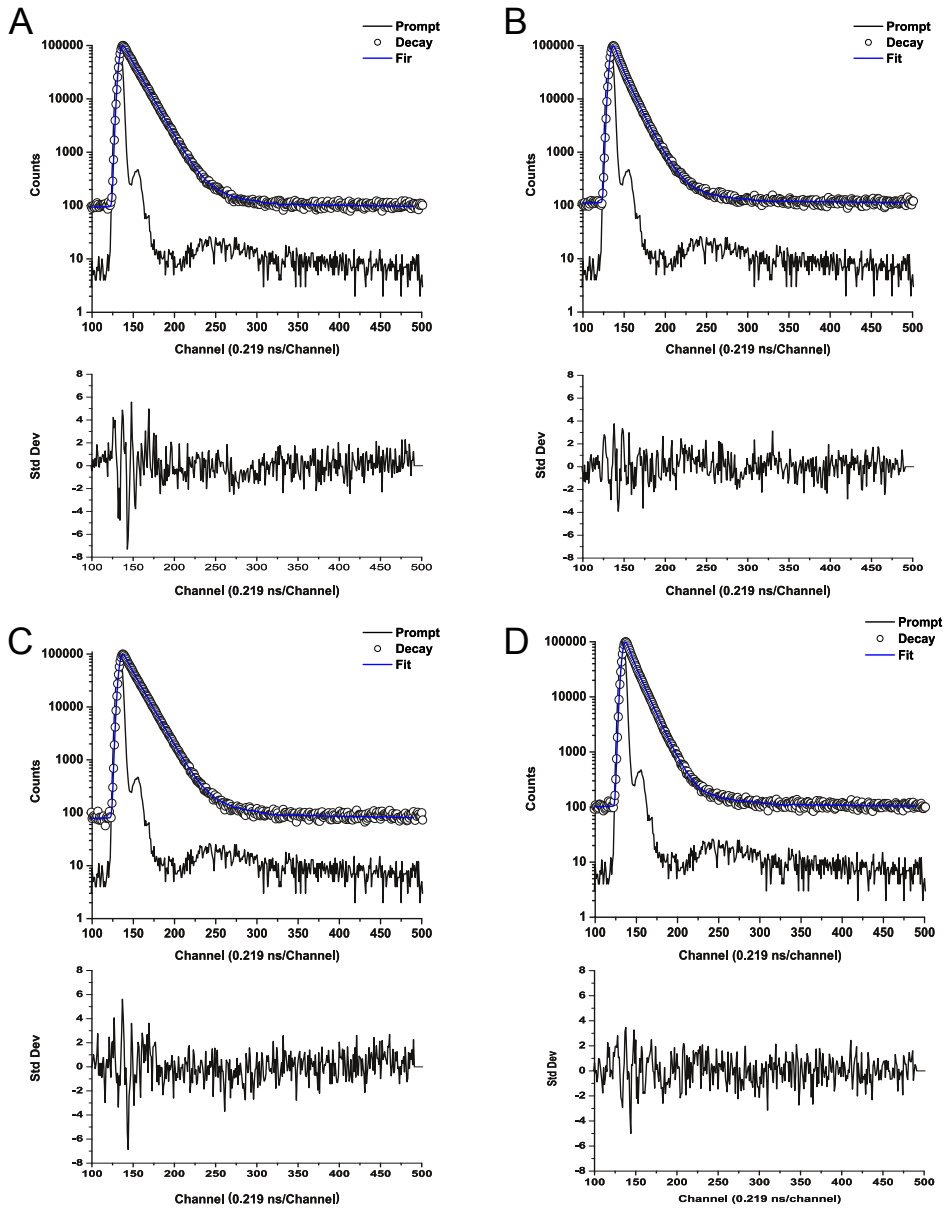

Figure 5: **Ensemble fluorescence lifetime measurements.** Lifetime decay data and fits are plotted for A: Atto 532 in the absence of Atto 647N on a dsDNA13mer, B: Atto 532 in the presence of Atto 647N on a dsDNA13mer, C: Atto 532 in the absence of Atto 647N on a dsDNA15mer, D:Atto 532 in the presence of Atto 647N on a dsDNA15mer.

is tabulated in Table T1. Both the dsDNA13mers and 15mers labeled with Atto 532 showed to two lifetimes. Including a second lifetime resulted in at least a 1.5 fold reduction the reduced chi-square. While, the majority of the population (93%) decayed with a lifetime of 3.5 ns, there was a small population ($<$ 10%) of donor labeled 13mer and 15mer exhibiting lifetimes of 1.7 ns and 0.77 ns, respectively. Similar distributions of donor lifetimes were observed using single stranded preparations of the same labeled oligonucleotides (data not shown). No further improvement in fit could be obtained by including a third lifetime component. As described previously[14] the detection of multiple lifetimes of decay indicates that differential dye-nucleotide interactions may place the Atto 532 fluorophore in distinct environments. Different energy transfer efficiencies resulting from different spectroscopic properties of the dye in these environments could be responsible for the minor peaks observed in the histograms of ETE in Figure 4. Atto 647N attached to the nucleotides exhibited only a single lifetime of 4.3 ns (data not shown)

Sample	$t_1(ns)$	$t_2(ns)$	$t_3(ns)$	$Pop_1\%$	$Pop_2\%$	$Pop_3\%$	χ^2
13mer-DU	1.7	3.5	-	7.2	92.8	-	1.9
13mer-DA	1.9	3.5 (fixed)	0.6	47.8	44.9	7.3	1.4
15mer-DU	0.8	3.4	-	4.5	95.5	-	1.7
15mer-DA	2.3	3.4 (fixed)	0.7	57.8	34.1	8.1	1.4

Table T1: Ensemble fluorescence lifetime data. Lifetime data for double stranded DNA that only has a donor (DU), for double stranded DNA that is labeled with a donor and an acceptor (DA) and for double stranded DNA that is only labeled with an acceptor (AU). 'D' indicates donor strand. 'A' indicates acceptor strand and 'U' indicates unlabeled strand. The lifetime components are $t_1(ns)$, $t_2(ns)$ and $t_3(ns)$ and the relative amplitude of each lifetime in the fit is given by the population numbers $Pop_1\%$, $Pop_2\%$ and $Pop_3\%$. The χ^2 value shows the goodness of fit.

The population distributions of Atto 532 dyes exhibiting different lifetimes in the presence of the Atto 647N acceptor were significantly different from what was observed for molecules labeled with donor alone. Fitting the decays with three lifetimes provided a significant improvement over the quality of the fit obtainable with two components from a reduction in chi squared from 1.75 to 1.35 for the dsDNA13mer, and from 1.73 to 1.42 for the dsDNA15mer. Including a fourth lifetime did not provide any further improvement of the fits. Since the sample preparation procedure did

not include a step to remove the single stranded donor and acceptor strands, the sample contained a significant population of single-stranded molecules containing only the donor dye. Thus in fitting the decays of samples containing both donor and acceptor, the unquenched lifetime was fixed at 3.5 ns for dsDNA13mer and 3.4 ns for dsDNA15mer, the value measured for the predominant population of decays in samples containing donor-only molecules.

For donor- and acceptor-labeled dsDNA13mer, the population of decays exhibiting a lifetime of 3.5 ns decreased to less than 50% and two additional lifetimes of 1.9 and 0.6 ns were derived from the fitting. The 1.9 ns population, representing about 45% of the population, is most likely dominated by double stranded molecules undergoing energy transfer, but is also likely to contain a small contribution ($<$ 5% of total molecules) from the shorter lifetime observed for single stranded molecules lacking acceptor. Just considering the decrease in lifetime of the major population from 3.5 to 1.9 ns, yields a calculated ETE of 0.45, corresponding to a donor-acceptor distance of 61 Å(based on an R_0 value of 59 Å). The small population of 13mers with the shortest lifetime ($<$ 10%) may be comprised of molecules with the shorter donor lifetime in which the decay is further accelerated by energy transfer. Similar consideration of the decrease in lifetime of the major population of dsDNA15mers yields an ETE value 0.32, corresponding to a donor-acceptor distance of 67 Å.

Steady state fluorescence measurements

Steady state FRET measurements were performed on a Fluoromax-4 instrument using excitation and emission slit settings of 2 nm and a 550 nm long-pass filter in the emission path. The approach described by Clegg et al.[15] was used to calculate ETE based on a comparison of donor excitation and direct acceptor excitation for the same sample. Donor was excited at 500 nm. Direct excitation of acceptor was performed at 644 nm. After correcting for background and crosstalk (using13mer-

DU and 15mer-DU), ETE was calculated using the following equation

$$ETE = [\frac{F_{500\ nm}}{F_{644\ nm}} - \frac{\varepsilon^{A}{}_{500\ nm}}{\varepsilon^{A}{}_{644\ nm}}]\frac{\varepsilon^{A}{}_{644\ nm}[A^{+}]}{\varepsilon^{D}{}_{500\ nm}[d^{+}a^{+}]}\ , \tag{9}$$

where $F_{500\ nm}$ is the integrated area under the emission spectrum from 655 nm - 800 nm with 500 nm excitation, $F_{644\ nm}$ is the integrated area under the emission spectrum from 655 nm - 800 nm with 644 nm excitation, $\varepsilon^{A}_{500\ nm}$ is the extinction coefficient of the acceptor at 500 nm (405 $lM^{-1}cm^{-1}$ for dye attached to 13mer and 385.5 $lM^{-1}cm^{-1}$ for dye attached to 15mer) $\varepsilon^{A}_{644\ nm}$ is the extinction coefficient of the acceptor at 644 nm (150,000 $lM^{-1}cm^{-1}$), $\varepsilon^{D}_{500\ nm}$ is the extinction coefficient of the donor at 500 nm (37,100 $lM^{-1}cm^{-1}$ for dye attached to 13mer and 35,900 $lM^{-1}cm^{-1}$ for dye attached to 15mer),$[A^{+}]$ is the total acceptor strand concentration, and $[d^{+}a^{+}]$ is the fraction of the acceptor strand that is double stranded. The extinction coefficient of donor at 532 nm and acceptor at 644 nm were obtained from the website of the supplier (Atto-Tec, Germany). The extinction coefficients at 500 nm for the two dyes were obtained by measuring

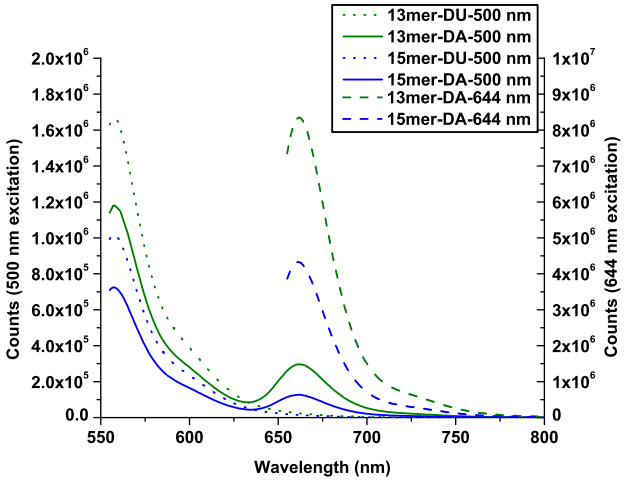

Figure 6: **Steady state fluorescence:** Background subtracted emission spectra with 500 nm excitation (left y-axis) are plotted for : 13mer-DU-500 nm (olive dotted curves), 13mer-DA-500 nm (olive solid curve), 15mer-DU-500 nm (blue dotted curve), 15mer-DA-500 nm (blue solid curve). Background subtracted emission spectra with 644 nm excitation (right y-axis) are plotted for: 13mer-DA-644 nm (olive dashed curve), 15mer-DA-644 nm (blue dashed curve).

emission spectra of the dyes attached to DNA at different excitation wavelengths.

Since the donor and acceptor strands are chemically synthesized and purified, each strand should be 100% labeled. $\frac{[d^+a^+]}{[A^+]}$ is the fraction of acceptor (Atto647N strand) that is hybridized with a donor-containing (Atto532) strand. This can be calculated based on the knowledge of the total concentration of the donor (4 μM) and acceptor strand (8 μM) and the fractional single stranded donor population calculated from the population of molecules retaining the longest decay time in the fluorescence lifetime measurements (A minor correction was also applied to account for the existence of the small population associated with a rapid decay time observed in lifetime measurements of single stranded labeled DNAs). As expected the fraction of hybridized molecules was higher for the 15mer (0.32) than for the 13mer (0.26). Using these numbers, the ETE of the 13mer was calculated to be 0.51, while the ETE for the 15mer was 0.35, corresponding to donor-acceptor distances of 59 Åand 65 Å, respectively, in good agreement with the ETE values measured for the same samples using fluorescence lifetime.

References

(1) Nir, E.; Michalet, X.; Hamadani, K. M.; Laurence, T. A.; Neuhauser, D.; Kovchegov, Y.; Weiss, S. Shot-Noise Limited Single-Molecule FRET Histograms: Comparison between Theory and Experiments. *J Phys Chem B* **2006**, *110*, 22103–22124.

(2) Zhang, K.; Yang, H. Photon-by-Photon Determination of Emission Bursts from Diffusing Single Chromophores. *J. Phys. Chem. B* **2005**, *109*, 21930–21937.

(3) Fu, D.; Sarker, R.; Abe, K.; Bolton, E.; Maloney, P. Structure/function relationships in OxlT, the oxalate-formate transporter of oxalobacter formigenes. II: Assignment of transmembrane Helix 11 to the translocation pathway. *J. Biol. Chem.* **2001**, *276*, 8753–8760.

(4) Fu, D.; Maloney, P. Structure/function relationships in OxlT, the oxalate-formate transporter of oxalobacter formigenes. I: Topological features of trans-membrane Helix 11 as visualized by site-directed fluorescent labeling. *J. Biol. Chem.* **1998**, *273*, 17962–17967.

(5) Abe, K.; Ruan, Z. S.; Maloney, P. C. Cloning, sequencing and expression in Escherichia coli of OxlT, the oxalate/formate exchange protein of Oxalobacter formigenes. *J. Biol. Chem.* **1996**, *271*, 6789–6793.

(6) Dave, R.; Terry, D. S.; Munro, J. B.; Blanchard, S. C. Mitigating Unwanted Photophysical Processes for Improved Single-Molecule Fluorescence Imaging. *Biophysical Journal* **2009**, *96*, 2371.

(7) Aitken, C. E.; Marshall, R. A.; Puglisi, J. D. An Oxygen Scavenging System for Improvement of Dye Stability in Single-Molecule Fluorescence Experiments. *Biophysical Journal* **2008**, *94*, 1826.

(8) Min, H.; Joo, Y.; Song, O. Effects of Wafer Cleaning and Annealing on Glass/Silicon Wafer Direct Bonding. *J. Electron. Packag* **2004**, *126*, 120–123.

(9) Fokker, A. D. Die mittlere Energie rotierender elektrischer Dipole im Strahlungsfeld. *Annalen der Physik* **1914**, *43*, 810–820.

(10) Planck, M. Über einen Satz der statistichen Dynamik und eine Erweiterung in der Quantumtheorie. *Sitzungberichte der Preussischen Akadademie der Wissenschaften* **1917**, 324–341.

(11) Kohler, R. H.; Schwille, P.; Webb, W. W.; Hanson, M. R. Active protein transport through plastid tubules: velocity quantified by fluorescence correlation spectroscopy. *J Cell Sci* **2000**, *113*, 3921–3930.

(12) Pennathur, S.; Santiago, J. G. Electrokinetic Transport in Nanochannels. 1. Theory. *Anal. Chem.* **2005**, *77*, 6772–6781.

(13) Hoogenboom, J. P.; Hernando, J.; van Dijk, E. M. H. P.; van Hulst, N. F.; Garcia-Parajo, M. F. Power-Law Blinking in the Fluorescence of Single Organic Molecules. *Chemphyschem* **2007**, *8*, 823–833.

(14) Iqbal, A.; Arslan, S.; Okumus, B.; Wilson, T.; Giraud, G.; Norman, D.; Ha, T.; Lilley, D. Orientation dependence in fluorescent energy transfer between Cy3 and Cy5 terminally attached to double-stranded nucleic acids. *Proc. Natl. Acad. Sci. USA* **2008**, *105*, 11176.

(15) Clegg, R. M. Fluorescence resonance energy transfer and nucleic acids. *Methods in Enzymology* **1992**, *211*, 353.